THE JOURNAL OF PHYSICAL CHEMISTRY C

Article

Cite This: J. Phys. Chem. C 2019, 123, 18939−18950

pubs.acs.org/JPCC

Well-Ordered Monolayer Growth of Crown-Ether Ring Molecules on Cu(111) in Ultra-High Vacuum: An STM, UPS, and DFT Study

Ryohei Nemoto,[†] Peter Krüger,[†,‡] Ayu Novita Putri Hartini,[†] Takuya Hosokai,[§] Masaki Horie,[∥] Satoshi Kera,[†,⊥] and Toyo Kazu Yamada*[,†,‡]

[†]Department of Materials Science, Chiba University, 1-33 Yayoi-cho, Inage-ku, Chiba 263-8522, Japan

[‡]Molecular Chirality Research Center, Chiba University, 1-33 Yayoi-cho, Inage-ku, Chiba 263-8522, Japan

[§]National Metrology Institute of Japan, National Institute of Advanced Industrial Science and Technology, Tsukuba Central 2, 1-1-1 Umezono, Tsukuba, Ibaraki 305-8568, Japan

[∥]Department of Chemical Engineering, National Tsing Hua University, 101, Sec. 2, Kuang-Fu Road, Hsinchu, 30013, Taiwan

[⊥]Institute for Molecular Science, Myodaiji, Okazaki 444-8585 Japan

Supporting Information

ABSTRACT: Crown-ether (CR) ring molecules are known as host molecules for capturing guest species inside the ring. So far CR molecular films have only been grown by drop-casting a CR solution on an inert substrate in air which offers little control over the molecular structure. Here we report the successful growth of a well-ordered CR molecular array on an atomically flat and clean noble metal Cu(111) substrate at 300 K in ultra-high vacuum (UHV), using 4,4′,5,5′-tetrabromodibenzo[18] crown-6 ether (Br-CR). The adsorption, self-assembly, and electronic structures of Br-CR were studied by means of UHV low-temperature scanning tunneling microscopy and spectroscopy, low electron energy diffraction, and angle-resolved ultraviolet photoemission spectroscopy. We found that (1) the Br-CR ring, which is bent both in the crystal and gas phase, flattens upon adsorption on Cu(111). Density functional theory reveals that the two benzene groups of the molecule lie flat on the surface such as to maximize the substrate-molecule interaction. (2) The moderate molecule−substrate interaction allows thermal diffusion of the Br-CR molecules, resulting in the formation of self-assembled monolayer islands with 7 × 4 superstructure. (3) While the deposition of 0.05 ML Br-CR forms multidomain islands with disordered defects, a drastic improvement occurred at 0.25 ML, where only atomically flat single-domain islands were grown. This Br-CR flat ring cavity array could become a template for designing novel two-dimensional arrays of desired guest atoms, ions, or functionalized molecules.

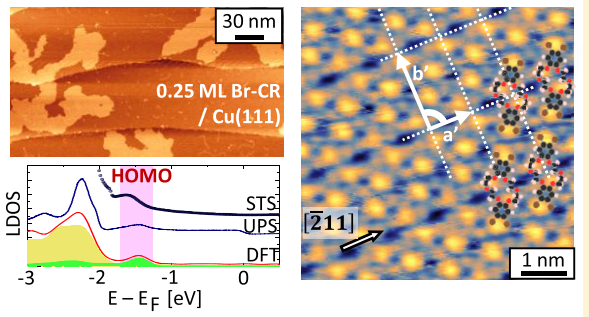

1. INTRODUCTION

The growth of organic films by molecular evaporation and deposition on atomically clean substrates in ultrahigh vacuum (UHV) has been studied intensively in the last decades.[1−16] UHV growth has several advantages with respect to chemical growth methods such as drop-casting a molecular solution on the substrate in air.[17−20] First, contamination of the film with solvent residue, a common problem with solution-based processes, is excluded in UHV. Second, the formation of well-ordered molecular arrays can be controlled more easily in molecular beam epitaxy under UHV conditions, because of the cleanliness of the substrate and control of deposition rate and substrate temperature. As a consequence, molecular films grown in UHV contain much fewer defects due to impurities, improving the molecular crystallinity, electronic properties and thus the device quality.[21]

Since atomically flat and clean (impurity <1%) substrate surfaces are obtained in UHV, new novel molecular nanostructures can be designed using the atomic precise control of the substrate surface crystalline structures. So far, UHV growth of two-dimensional molecular arrays has mainly focused on flat plane π-conjugated organic molecules, such as phthalocyanine (Pc), porphyrin (TPP), pentacene, perylene-tracarboxylic dianhydride (PTCDA), and tetracyanoquinodimethane (TCNQ).[1−16] These rigid molecules are not deformed or deconstructed during the sublimation and heating to 400−600 K, which allows for controllable sublimation from molecular powders in an aluminum or quartz crucible in UHV. On atomically flat noble metal substrates, such flat, π-conjugated molecules can self-assemble into well-ordered arrays.

Crown-ether (CR) cyclic ring molecules are known[22−33] for their ability to capture guest metal atoms, ions, or molecules inside the ring. Therefore, CR molecular films are very

Received: April 10, 2019
Revised: June 25, 2019
Published: July 15, 2019

Downloaded via CHIBA UNIV on August 9, 2019 at 01:55:51 (UTC).
See https://pubs.acs.org/sharingguidelines for options on how to legitimately share published articles.

© 2019 American Chemical Society

DOI: 10.1021/acs.jpcc.9b03335
J. Phys. Chem. C 2019, 123, 18939−18950

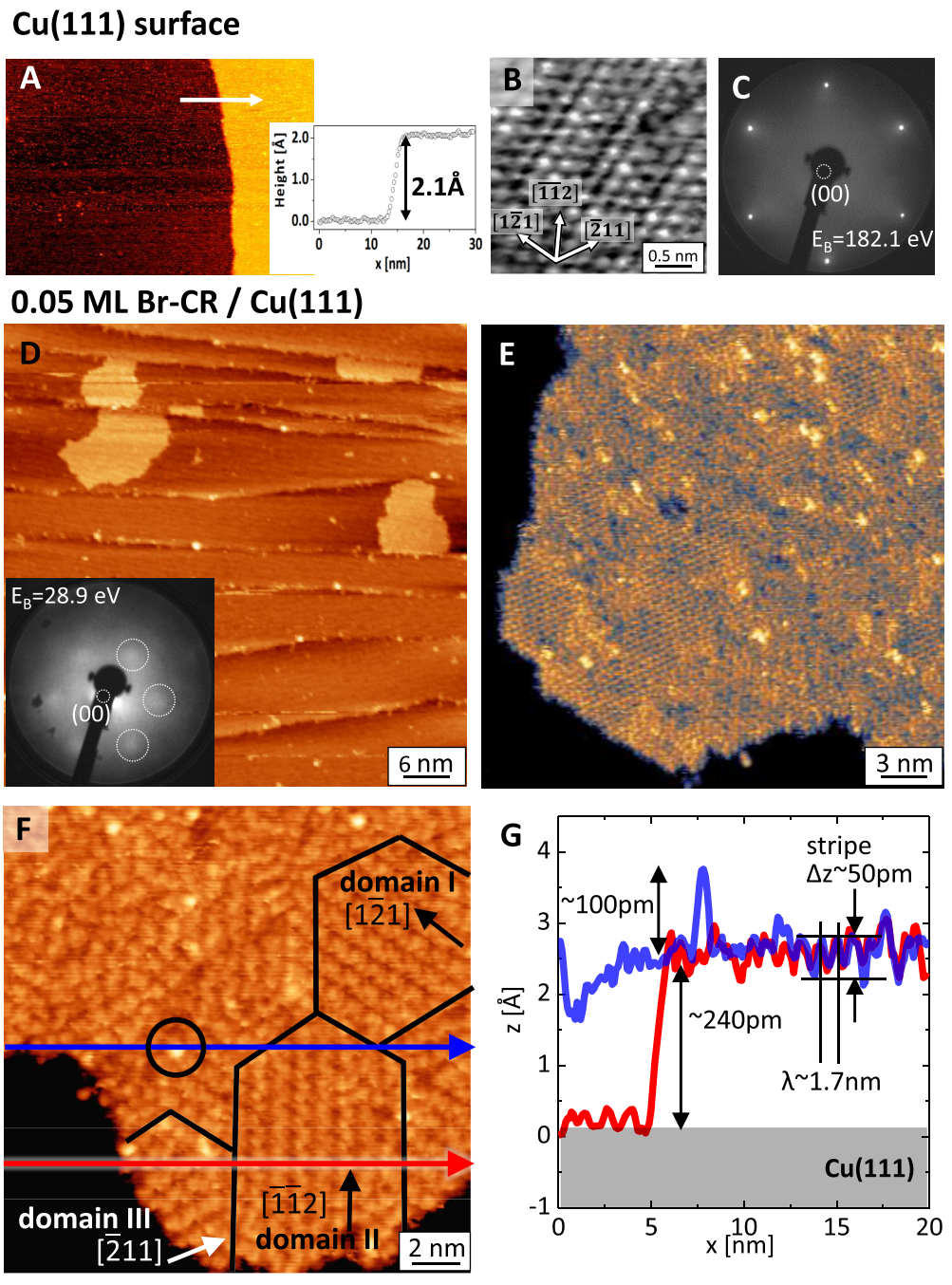

Figure 1. STM/LEED results obtained on bare Cu(111) surface and 0.05 ML Br-CR on Cu(111). (A) STM image obtained on a clean Cu(111) atomic terraces (100 × 70 nm^2, V_s = −1.0 V, I_t = 300 pA). Line profile along the arrow shows the step height of ~210 pm in good agreement with fcc-Cu(111) layer distance of 208 pm. (B) Atomically resolved STM image and (C) LEED spots (beam energy: 182.1 eV) obtained on the Cu terrace. Cu atoms follow the fcc(111) hexagonal symmetry. (D−F) STM images obtained on the Cu(111) surface covered by a 0.05 ML Br-CR: (D) 60 × 60 nm^2, V_s = +1.0 V, I_t = 20 pA, (E) 30 × 30 nm^2, V_s = −0.7 V, I_t = 100 pA, (F) 20 × 20 nm^2, V_s = −0.7 V, I_t = 100 pA. The inset in (D) denotes LEED spots obtained on the surface. Beam energy of 28.9 eV was used. White circles denote new 6-fold symmetry spots appeared after 0.05 ML Br-CR deposition. In (F), three domains were observed in one island. The stripe pattern in each domain follows the ⟨211⟩ direction. (G) Line profiles along the blue and red arrows in (F).

promising template materials for creating atomically controlled networks of captured guest species, in view of low-dimensional device applications.[33−42]

However, CR ring molecules are more delicate for UHV growth than the aforementioned flat π-conjugated molecules, because the CR ring is soft and flexible, i.e., it can easily be deformed and possibly deconstructed during the sublimation and heating process involved in UHV growth. We note that in all previous reports on UHV measurements of CR molecular films, the films were grown by drop-casting the CR solution on an inert Au or highly oriented pyrolytic graphite (HOPG) surface.[26,31]

Here we demonstrate the successful UHV growth of a flat ring array using a 4,4′,5,5′- tetrabromodibenzo[18] crown-6 ether (Br-CR) on an atomically flat and clean Cu(111) substrate at 300 K. To the best of our knowledge, this is the

DOI: 10.1021/acs.jpcc.9b03335
J. Phys. Chem. C 2019, 123, 18939−18950

first demonstration of CR film growth under UHV conditions. Precise molecule crystalline structures were obtained using atomically resolved UHV scanning tunneling microscopy (STM) and high-sensitive low-energy electron diffraction (LEED). Further, the electronic state of the array was analyzed using scanning tunneling microscopy (STS) and angle-resolved ultraviolet photoemission spectroscopy (UPS). Experimentally obtained crystalline and electronic structures of the ring array were successfully reproduced by density functional theory (DFT) calculations, and the energetically most stable molecular structure was identified.

In this work, we show that (1) the Br-CR ring, which is bent both in the crystal and gas phase, adopts a flat conformation upon adsorption on Cu(111). DFT reveals that the two benzene groups of the molecule are parallel to the surface such as to maximize the substrate-molecule interaction. (2) The moderate molecule−substrate interaction allows thermal diffusion of the Br-CR molecules, resulting in the formation of self-assembled monolayer islands with a 7 × 4 periodicity on Cu(111). (3) While the deposition of 0.05 ML Br-CR forms multidomain islands with disordered defects, a drastic improvement occurs at 0.25 ML, where atomically flat single-domain islands are obtained.

2. METHODS

2.1. Low-Temperature UHV STM Setup. STM/STS measurements were performed by using a home-built apparatus (see Supporting Information, SI Figure S1), which consists of STM (No.1 in Figure S1B), preparation (No.2), and deposition chambers (No.3). All chambers have a base pressure below 2.0×10^{-8} Pa. Tips and samples were transferred between chambers using transfer rods without breaking the UHV. Each chamber was separated by gate valves. A UHV cryostat (CryoVAC) located on the STM chamber was used to cool down the whole STM setup. We filled liquid nitrogen for both inner and outer tanks in the cryostat. STM/STS measurements were performed at 78 K in UHV. STM probe tips and samples were introduced by opening only the deposition chamber (No.3).

2.2. W Tip Probe. Tungsten tips were used as a probe. A tungsten wire (diameter 0.3 mm, purity 99.95%) was chemically etched with aqueous KOH solution (~2 N) in air, and subsequently rinsed by hot water and acetone. The apex was monitored by scanning electron microscopy (10^{-2} Pa, Tiny-SEM, Technex Co., Ltd.). Only sharp cone-shape tips were introduced into the preparation chamber (No.2, see SI Figure S1B). Proper flashing treatments were performed in the preparation chamber to remove the oxide film coating on the W tip apex.[43] A clean and sharp W tip was set into the STM head in the STM chamber (No.1).

2.3. Cu(111) Substrate. We used two Cu(111) single crystals, one for UPS/LEED and another one for STM. Both Cu(111) single crystals (diameter 6 mm, MatecK, 99.999%) were carefully sputtered and annealed to obtain clean and atomically flat surfaces (see Figure 1A−C and Supporting Information, SI Figure S2).[44] Cleaning parameters were Ar^+ sputtering (+1.0 keV, 420 nA, Ulvac PHI floating type ion gun) and annealing (~820 K) for the STM setup, and Ar^+ sputtering (+1.0 keV, 600 nA) and annealing (~770 K) for the UPS setup. During the sputtering, the pressure around the sample was maintained below 3.0×10^{-8} Pa by differential pumping. Br-CR molecules were deposited on the clean and atomically flat Cu(111) surface in the introduction chamber. The crystal orientation of the Cu(111) substrate was obtained by measuring the STM atomic image (see Figure 1B) and LEED spots (see Figure 1C). Scanning tunneling spectroscopy (STS) showed the surface state peak at −0.35 eV and angle-resolved UPS also showed the s-band surface state peak around −0.4 eV and d-band peak at −2.3 eV (see SI Figures S2 and S4).

2.4. STM and STS Measurements. A home-built STM combined with the Nanonis SPM controller BP4 was used to obtain topographic images of sample surfaces in a constant current mode. Since the tunneling current (I) detected by the tip is exponentially proportional to the tip−sample separation (z) via $\exp[-8m(\Phi \pm eV_s/2)\, z\, /\hbar]$, where m: electron mass, $\hbar$: Planck constant, Φ: apparent barrier height between tip and sample, and V_s: set point sample bias voltage, we can measure the surface corrugations in the order of 1 pm.

STS can measure sample surface local density of states (LDOS). Tunneling current (I) as a function of sample bias voltages (typically, from −2 V to +2 V) was measured under feedback off condition (one single curve was measured within 50−200 ms) by fixing the tip−sample separation ($z = z_c$), which was determined by the set point voltage ($V = V_s$) and the current ($I = I_s$). The obtained $I(V)$ curves were numerically differentiated, and differential conductance (dI/dV) curves were obtained: $dI/dV = \rho \cdot \exp[-8m(\Phi \pm eV_s/2)\, z\, /\hbar]$, where ρ denotes sample surface LDOS. The obtained STM/STS data were analyzed using WSxM 5.0 Develop 9.0 software[45] and Gwyddion 2.53.

2.5. UHV, ARUPS, and LEED Measurements. UPS and LEED measurements were conducted in the home-built UHV apparatus (see SI Figures S1, S4, and S7). The angle-resolved UPS (ARUPS) and angle-integrated UPS were performed at 295 K using an ultralow-background, high-sensitivity UPS apparatus with a hemispherical electron energy analyzer (MBS-A-1) and two monochromators (MBS-M-1) for two wavelength regions as setup in the SI Figure S1A. The first one is for HeIα ($h\nu$ = 21.218 eV) and HeIIα ($h\nu$ = 40.814 eV) radiation sources by a high-density plasma lamp (MBS-L1) with Al filter. The second one covers the low-photon energy range, and XeIα ($h\nu$ = 8.437 eV) is used as a radiation source by a capillary discharge lamp (Omicron HIS13) with a LiF single-crystal filter.[46]

The Cu(111) was cleaned at the preparation chamber (<5.0×10^{-8} Pa), and Br-CR molecules were deposited in the deposition chamber (<6.0×10^{-7} Pa). LEED with a multichannel plate (MCP) equipped in the preparation chamber was used to detect weak electron signal from the monolayer molecular film (see Figure 2). To avoid damages to the deposited molecular film, we used 10−40 eV beam energy. High-resolution spot-profile analysis LEED (SPA-LEED) was performed for the annealed film (see SI Figure S7). UPS was measured in the chamber No.1 (<1.0×10^{-8} Pa) in SI Figure S1A. ARUPS spectra were measured with an acceptance angle of ±18° (see SI Figure S4). Angle-integrated UPS spectra were recorded by a transmission (spatial) mode. The total instrumental energy resolution of the measurements was set to 30 meV. A bias of −5 V was applied to the sample in order to detect the secondary cutoff. The binding energy scale is referred to the Fermi level (E_F) measured on a metal substrate.

2.6. Br-CR Sublimation Control in UHV. We used two different UHV setups: one for ARUPS and LEED, and another one for low-temperature STM (see SI Figure S1). Therefore, it was necessary to control precisely the amount of deposited

DOI: 10.1021/acs.jpcc.9b03335
J. Phys. Chem. C 2019, 123, 18939−18950

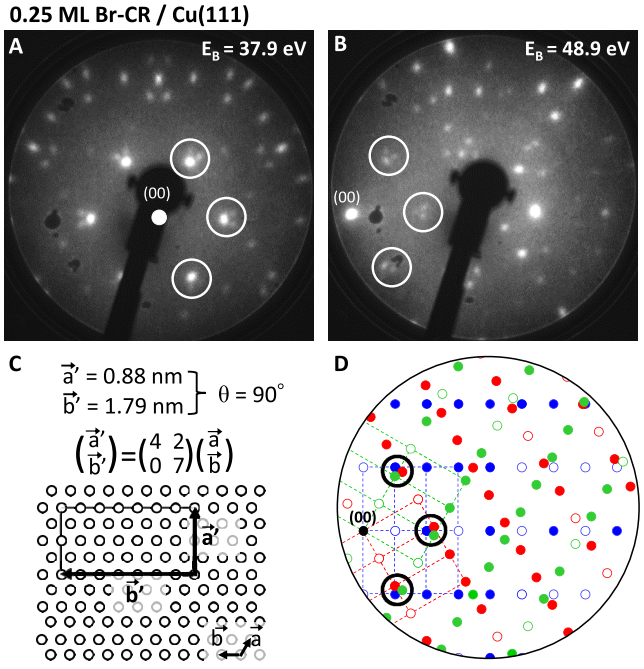

Figure 2. LEED results obtained on 0.25 ML Br-CR on Cu(111). (A, B) LEED spots obtained by illuminating beam energy of (A) 37.9 eV and (B) 48.9 eV. White circles denote new 6-fold symmetry spots appeared after 0.25 ML Br-CR deposition. In the circle, three spots are observed. (C) A unit cell obtained from the LEED spots in (A, B): $\vec{a}$= 0.88 nm, $\vec{b}$ = 1.79 nm, θ = 90°. (D) Simulated LEED spots using the unit cell in (C). Blue, green, and red dots correspond to each domain in Figure 1F. These spots well reproduced three spots in the circles in (A, B).

molecules on the Cu(111) substrate at 300 K in both setups. We used the same quartz SiO_2 crucible and the same home-built molecular evaporator (thermal radiation heating) to obtain the same crucible temperature and the same pressure (1×10^{-6} Pa, see SI Figure S1C,D). For the quartz crystal microbalance (QCM), the same parameters (z-ratio = 1, density = 1) were taken to operate QCM and set QCM at the same distance from the crucible (110 mm). The quarts crucible was radiatively heated by flowing current through a tungsten wire filament (diameter 0.3 mm). The crucible temperature was monitored by using the almel-chromel thermocouple contacting to the bottom of the crucible. The Cu(111) substrate was put ∼110 mm above the crucible. Before the deposition, we always checked the Br-CR evaporation rate by setting a QCM at the same distance position. SI Figure S1E shows one example of the obtained QCM data. We carefully increased the crucible temperature in time, and exactly above the crucible temperature of 84.0 °C (∼357 K), QCM detected the molecule deposition. From the slope in Figure S1E, the evaporation speed of 0.03 nm/min and 0.08 nm/min were reproducibly obtained at the crucible temperature of 87.6 °C (∼361 K) and 95.9 °C (∼369 K), respectively. We used the former evaporation rate. Since the QCM parameters of z-ratio and molecule density, the estimated deposition amounts as well as the adsorption probability on the substrate were unknown, the molecule thickness estimated by QCM was only used as an index. Precise deposited molecular monolayer (ML) was checked by STM.

2.7. Synthesis of 4,4′,5,5′-Tetrabromodibenzo[18]-crown-6 Ether (Br-CR). Br-CR was prepared according to modification of the literature method.[47] In a 500 mL three-necked flask with a reflux condenser connected to a gas absorption trap, a mixture of bromine (3.92 g, 24.5 mmol) and acetic acid (25 mL) was added to a chloroform solution (300 mL) of dibenzo[18]crown-6 (2.00 g, 5.55 mmol) at room temperature. The mixture was refluxed for 12 h. After cooling, the orange powder was filtered and washed with diethyl ether (50 mL × 5 times) to give a white powder. This was purified by recrystallization from methanol solution to afford Br-CR as white crystals (1.4 g, 50%). Anal. Calcd for $C_{20}H_{20}Br_4O_6$: C, 35.54; H, 2.98; Br, 47.28%. Found: C, 35.47; H, 2.96; Br, 47.10%. ^{1}H NMR (400 MHz, $CDCl_3$, r. t.): δ 3.96 (t, 8H, CH_2, J(HH) = 4.4 Hz), 4.11 (t, 8H, CH_2, J(HH) = 4.4 Hz), 7.05 (s, 4H, aromatic). FABMS: m/z = 676 $[M]^+$. CCDC 1901496 contain the supplementary crystallographic data for this paper. These data can be obtained free of charge via www.ccdc.cam.ac.uk/data_request/cif, or by emailing data_request@ccdc.cam.ac.uk, or by contacting The Cambridge Crystallographic Data Centre, 12 Union Road, Cambridge CB2 1EZ, UK; fax: + 44 1223 336033.

2.8. DFT Calculations. Density functional theory (DFT) calculations with the PBE exchange-correlation potential were performed using the VASP code (see SI Figures S5 and S6).[48] The plane-wave energy cutoff was 400 eV and the k-point spacing was about 0.2 Å^{-1} (e.g., 3 × 5 × 1 k-mesh for a 17.8 × 8.8 × 25.0 Å unit cell). Dispersion corrections were included using the Grimme DFT-D2 scheme.[49] The C6 coefficient of Cu was reduced by 50% (to 5.4 J nm^6 mol^{-1}) to correct for the systematic overestimation of molecule−metal adsorption energy in DFT-D2.[50] With the chosen C6 value, the Cu bulk lattice constant (3.605 Å) and adsorption energy of benzene/Cu(111) (0.62 eV) are in excellent agreement with experiment (3.603 Å and 0.71 eV, respectively).[51] The Cu(111) substrate was modeled with a slab of four atomic layers separated by 17 Å of vacuum.[52] The atomic structure was optimized until all forces were below 0.01 eV/Å. The experimentally observed $\begin{pmatrix}\vec{a}'\\ \vec{b}'\end{pmatrix} = \begin{pmatrix}4 & 2\\ 0 & 7\end{pmatrix}\begin{pmatrix}\vec{a}\\ \vec{b}\end{pmatrix}$ surface cell was used for the Br-CR/Cu(111) system, where $\vec{a}$ and $\vec{b}$ denote the unit vectors on the Cu(111) substrate. STM pictures were simulated using the Tersoff-Hamann approximation with the experimental bias. For the density of states (DOS) plot, the partial Cu-d DOS was down-shifted by 0.5 eV to correct for the underestimation of the Cu-3d band binding energy in DFT.[53]

3. RESULTS AND DISCUSSION

In this study, we examined the adsorption and self-assembly of Br-CR ring molecules on an atomically flat Cu(111) substrate. To obtain a well-order molecular array, two conditions should be met. (1) The molecules have a defined adsorption geometry. (2) The surface diffusion barriers are low enough to enable rearrangement and self-assembly of the molecules. As a ring molecule, 4,4′,5,5′-tetrabromodibenzo[18] crown-6 ether (Br-CR) was used (see Methods 2.6 and 2.7). The Br-CR ring is known to be bent both in the crystal and gas phase (see SI Figure S1F). The Br-CR molecules were reproducibly sublimated with a stable deposition rate of 0.03 nm/min at a crucible temperature of 87.6 °C in UHV (see SI Figure S1E).

A choice of the substrate is crucial factor for the UHV on-surface growth since the energy balance between the

DOI: 10.1021/acs.jpcc.9b03335
J. Phys. Chem. C 2019, 123, 18939−18950

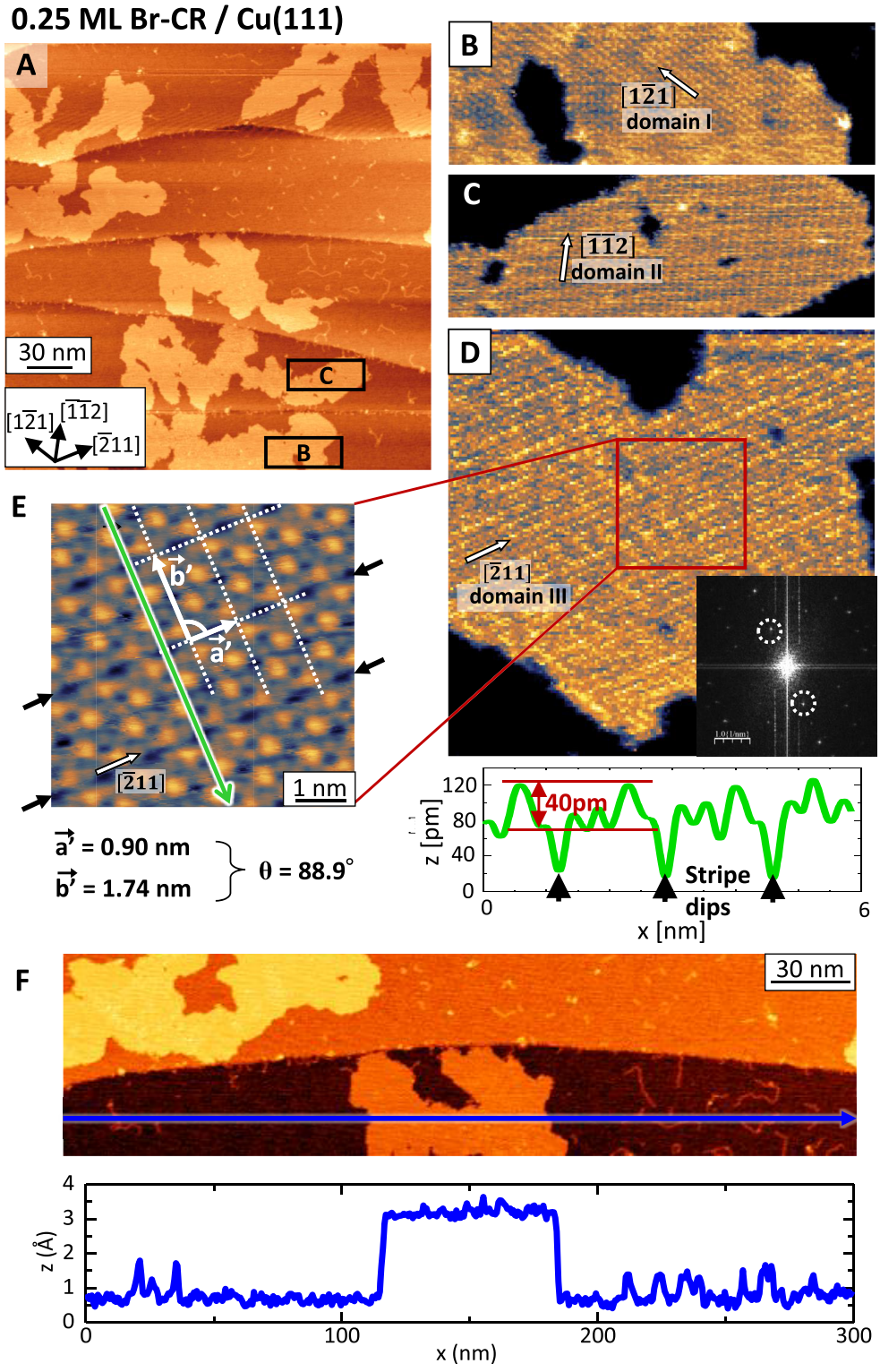

Figure 3. STM results obtained on 0.25 ML Br-CR on Cu(111). (A) STM topographic image (300 × 300 nm^2, V_s = −0.7 V, I_t = 10 pA). 25% of the Cu(111) surface was covered by the molecular islands. Here each island includes only one domain. (B, C) Enlarged images of the boxed areas in (A). From the stripe patterns domain I in (B) and domain II in (C) are identified. (D) STM image of the domain III island (30 × 30 nm^2, V_s = −0.7 V, I_t = 50 pA). The inset in (D) denotes the Fourier transformed image obtained from the STM image in (D). Clearly, two symmetric spots originated by the one-dimensional stripe pattern are observed. (E) Enlarged STM image obtained on the island in (D) (6 × 6 nm^2, V_s = −0.7 V, I_t = 100 pA). The stripe patterns are marked by the black arrows. A unit cell obtained from the STM image in (E): $\vec{a}$ = 0.90 nm, $\vec{b}$ = 1.74 nm, θ = 88.9° is shown. The line profile along the green arrow is shown at the right-hand side panel. (F) STM image (300 × 70 nm^2). Chains are observed. A line profile along the blue arrow is shown in the lower panel.

molecule−substrate interactions and the intermolecular interactions controls the molecular array nanostructure. Here, we used a Cu(111) surface. Indeed, the well-known inert Au(111) or HOPG(0001) surface could be suitable as a

DOI: 10.1021/acs.jpcc.9b03335
J. Phys. Chem. C 2019, 123, 18939−18950

substrate since these inert surfaces are energetically stable at room temperature in air, liquid, and UHV. One disadvantage is a weak molecule−substrate interaction, i.e., the adsorbed molecule property is similar to gas phase.[54] However, the Br-CR molecule we use here has the bent ring structure in the crystal and gas phase. Our idea is to use the stronger molecule−substrate interaction, which could flatten the ring when the Br-CR is adsorbed on the substrate surface. The noble metal Cu(111) surface, which has 3d and 4s bands in the vicinity of the Fermi energy, could provide stronger interactions than the molecule-Au(111) interaction. Also, the Cu(111) surface has no surface reconstruction, and the cleaning and annealing processes to obtain atomically flan clean (impurity <1%) are established.[44]

The good quality of the Cu(111) substrate can be seen on the STM image in Figure 1. The terrace width is >50 nm and the step height is ∼210 pm (Figure 1A), in agreement with the bulk (111) layer distance of 208 pm. On the enlarged image (Figure 1B) with atomic resolution, the ⟨211⟩ crystal axes are identified, and the impurity concentration was found below 1%. The surface was also checked by LEED and 6-fold fcc(111) spots were clearly observed (see Figure 1C).

3.1. Br-CR Films on Cu(111) at 0.05 ML Coverage. First, we deposited only 0.05 ML of Br-CR at 300 K to understand how the molecules adsorb on Cu(111) and whether they form islands via thermal diffusion. The electronic interactions (charge transfer, dipole, or van der Waals) between adsorbed molecules and the substrate govern the adsorption energy and diffusion barrier height. The subtle balance between these energy terms determines diffusion rates and directions and thereby the shapes of self-assembled molecular islands.

Figure 1D shows an STM image obtained on the Cu(111) surface after depositing 0.05 ML Br-CR (60 × 60 nm^2). Several atomic terraces from bottom to top, and molecular islands are observed. Typical island sizes are 10 × 10−30 × 30 nm^2 with a constant height of ∼240 pm. The growth of the monolayer height islands implies that the adsorbed Br-CR molecules can diffuse on the Cu substrate at 300 K, which suggests low diffusion barriers and weak molecule substrate bonding. Also, one might note that one edge of the islands always, even at different sizes, follows the Cu(111) monatomic step, which indicates that the island growth occurs from the descending or ascending step. When single Br-CR molecules are adsorbed on the terrace, they immediately diffuse. Since the islands were always located at the step edge, the step could have a larger potential barrier enough to generate the nucleation. This is the well-known Ehrlich-Schwoebel barrier for descending a step edge.[55] The LEED image obtained on the same surface (see the inset in Figure 1D) shows that sharp 6-fold LEED spots in Figure 1C which originated by the fcc-Cu(111) symmetry disappeared after deposition of 0.05 ML of Br-CR, while new bright spots marked by the circles can be observed.

We focus on one island to see the details of the molecular structure inside the island (see Figure 1E). We found some stripe patterns and several bumps in the island, i.e., at 0.05 ML, the island surface is not continuously flat and ordered.

Upon closer inspection, we found three domains (see Figure 1F). Domain I, II, and III have stripe patterns parallel to $[1\bar{2}1]$, $[\bar{1}12]$, and $[\bar{2}11]$ directions. Line profiles along the blue and red arrows in Figure 1F are shown in Figure 1G. The Br-CR islands have a constant height of ∼240 pm. The stripe pattern has an interval of ∼1.7 nm with ∼50 pm corrugation. Seven to eight stripe lines are included in one single domain.

Although molecules inside each domain follow in periodic order, molecules around the domain boundaries are disturbed, forming disordered areas. This imperfection in the island could be the origin of the broadening of the LEED spots depicted in Figure 1D. The bumps (∼100 pm higher than the island surface) marked by the circle in Figure 1F were located at the disordered domain boundary. The bump could be buckled Br-CR molecule or a cluster due to the stress between domains.

Summarizing the results of low (0.05 ML) deposition at 300 K, we found that Br-CR on Cu(111) forms monolayer islands via thermal diffusion. The monolayer shows three domains oriented along the <211> equivalent directions. The island surface is not uniform, but features some disorder and roughness, and the domain size is small (2−5 nm). These findings show the difficulty of growing a well-ordered ring array using soft crown ether molecules. However, a drastic change occurred when the amounts of deposited molecules was increased to 0.25 ML as shown in the following.

3.2. Br-CR Films on Cu(111) at 0.25 ML Coverage. Upon increasing the coverage of 0.25 ML, a drastic improvement of the Br-CR molecule alignment in the island was observed. Much sharper LEED spots are seen in Figure 2A (E_B = 37.9 eV) and B (E_B = 48.9 eV), in which 6-fold symmetry spots marked by circles are identical to the blunter spots in Figure 1D, but here inside one circle, additional two satellite spots are visible adjacent to the strong spot. A unit cell of the Br-CR molecules alignment was obtained by using the LEED spots in Figure 2A and B: $|\vec{a}'|$ = 0.88 nm, $|\vec{b}'|$ = 1.79 nm, θ = 90.0° (see Figure 2C), i.e., we found the Br-CR ordered array has a uniform periodic pattern of $\begin{pmatrix}\vec{a}'\\ \vec{b}'\end{pmatrix} = \begin{pmatrix}4 & 2\\ 0 & 7\end{pmatrix}\begin{pmatrix}\vec{a}\\ \vec{b}\end{pmatrix}$, where $\vec{a}$ and $\vec{b}$ denote the unit vectors on the Cu(111) substrate. By rotating this rectangular unit cell by 60° and 120° around the (00) spot, we recovered the experimentally obtained LEED spots as shown in Figure 2D, where filled circles mean observable spots in Figure 2A and B. Namely, the LEED spots tell us the existence of three domains on 0.25 ML Br-CR surface.

Figure 3A shows an STM topographic image (300 × 300 nm^2) obtained on the Cu(111) surface deposited by 0.25 ML Br-CR. Now the islands are much larger (>50 nm) compared to Figure 1D. One remarkable point of these islands is that, at 0.25 ML, only one type of the stripe pattern is observed inside one island (see Figure 3B−D), i.e., the islands are single domains. Also, no bump exists in the island, i.e., the island has a flat uniform well-ordered structure.

Figure 3B−D shows STM topographic images of three different islands consisting of domain I, II, and III, where stripe patterns parallel to $[1\bar{2}1]$, $[\bar{1}12]$, and $[\bar{2}11]$ directions, respectively. The Fourier transformed image obtained from the STM image in Figure 3D clearly shows two symmetric spots originated from the one-dimensional stripe pattern (see the inset in Figure 3D, marked by circles).

The regularity in the Br-CR molecule at 0.25 ML was confirmed by visualizing molecular structures inside the island. Figure 3E shows a high-resolution STM image. Stripe patterns on the island follow the $[\bar{2}11]$ direction, but now ordered bright spots are also observed. From the periodicity in the STM image, we obtained the unit cell of $|\vec{a}'|$ = 0.90 nm, $|\vec{b}'|$ = 1.74 nm, θ = 88.9° (see Figure 3E). These values are in

DOI: 10.1021/acs.jpcc.9b03335
J. Phys. Chem. C 2019, 123, 18939−18950

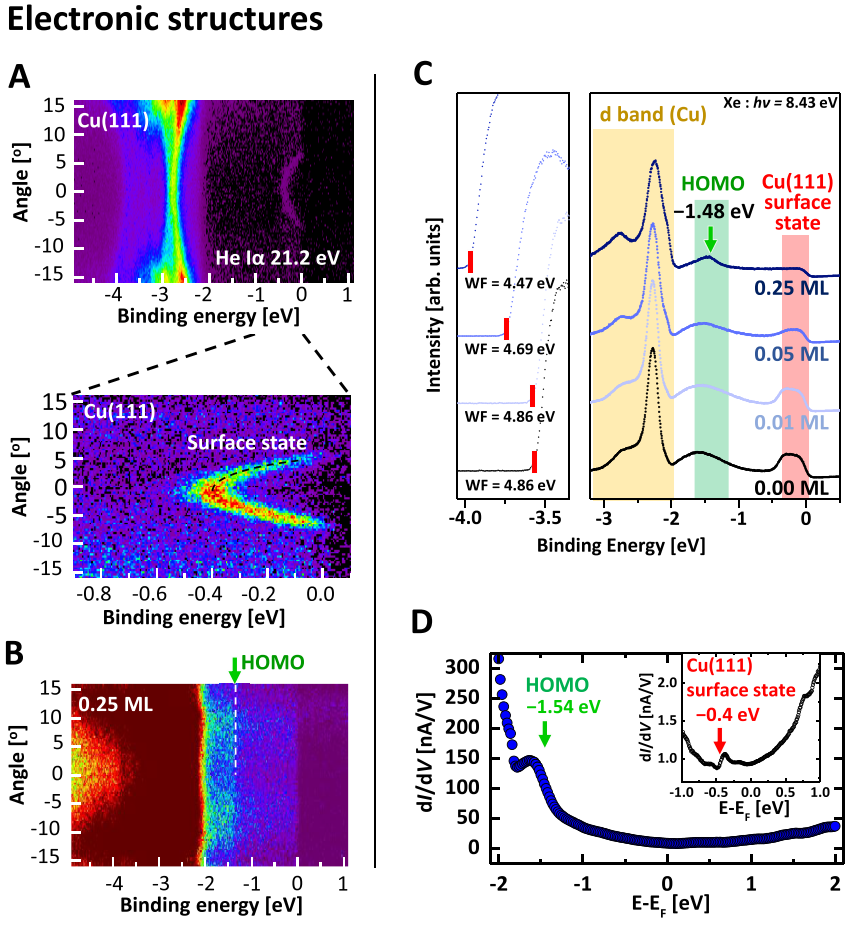

Figure 4. UPS and STS measurements for Br-CR on Cu(111). (A, B) Angle-resolved UPS results obtained on Cu(111) surface (A) before and (B) after the 0.25 ML Br-CR deposition. He Iα 21.2 eV light was used and the angle is measured from the surface normal. (C) Angle-integrated UPS results obtained at Br-CR coverages of 0.00, 0.01, 0.05, and 0.25 ML on Cu(111) with Xe 8.43 eV light. WF denotes work function. A new HOMO peak is appeared at −1.48 eV. (D) STS dI/dV curve obtained on the surface of 0.25 ML Br-CR on Cu(111). A HOMO peak is observed at −1.54 eV. The inset shows a dI/dV curve obtained on a bare Cu(111). The surface state peak at −0.4 eV is observed.

agreement with those obtained by LEED in Figure 2 ($|\vec{a'}|$ = 0.88 nm, $|\vec{b'}|$ = 1.79 nm, θ = 90.0°), where the same structure was obtained for the annealed monolayer film confirmed by SPA-LEED (Figure S7). In Figure 3E, one unit cell includes four bright protrusions, indicating that a single Br-CR molecule has four buckled positions. The flatness of the Br-CR array was checked by the line profile along the green arrow in Figure 3E, which shows that the stripe dips have a depth of ∼50 pm and the protrusions have a height of ∼40 pm. Namely, one Br-CR molecule has a corrugation within 40 pm. The line profile across the 80 nm-size island in Figure 3F clearly shows the flatness of the Br-CR array.

We note that apart from the monolayer islands, one-dimensional features are frequently observed on the terraces (see Figure 3F and SI Figure S3C). These features have constant height (∼100 pm) and a width of ∼2 nm, comparable with the size of a Br-CR molecule and might be made of single molecular chains.

From the experimentally obtained STM and LEED results in Figures 2 and 3, we found that the growth of 0.25 ML Br-CR on Cu(111) at 300 K in UHV provides atomically flat well-ordered ring molecular array with a unit of $\begin{pmatrix}\vec{a'}\\ \vec{b'}\end{pmatrix} = \begin{pmatrix}4 & 2\\ 0 & 7\end{pmatrix}\begin{pmatrix}\vec{a}\\ \vec{b}\end{pmatrix}$, where $\vec{a}$ and $\vec{b}$ denote the unit vectors on the Cu(111) surface.

In order to better understand the electronic coupling between the adsorbed molecules and the substrate as well as between the molecules in the monolayer, we have performed in situ photoemission measurements. In particular, we checked whether the periodic arrangement of the molecules leads to band dispersion of the molecular levels and their position with respect to substrate bands.

Figure 4A shows angle resolved UPS maps of the bare Cu(111) surface measured with He Iα light (21.2 eV). The binding energy at 0 eV corresponds to the Fermi energy.

Cu 3d-bands around −2.5 eV and the parabolic band originated from the 4s surface state are clearly observed. We also checked with He IIα light (40.8 eV) since the molecular states may appear clearly using more than He Iα laser. We measured UPS with not only the angles between ±15° but also from 5° to 35° to see sp band (see Figure S4B).

The UPS map changes significantly upon deposition of 0.25 ML Br-CR (Figure 4B). We measured ARUPS using both He Iα and He IIα light (see Figures 4B and SI S4C for He Iα and SI S4D for He IIα). In particular, the surface state has disappeared and a slight increase of the intensity around −1.5

DOI: 10.1021/acs.jpcc.9b03335
J. Phys. Chem. C 2019, 123, 18939−18950

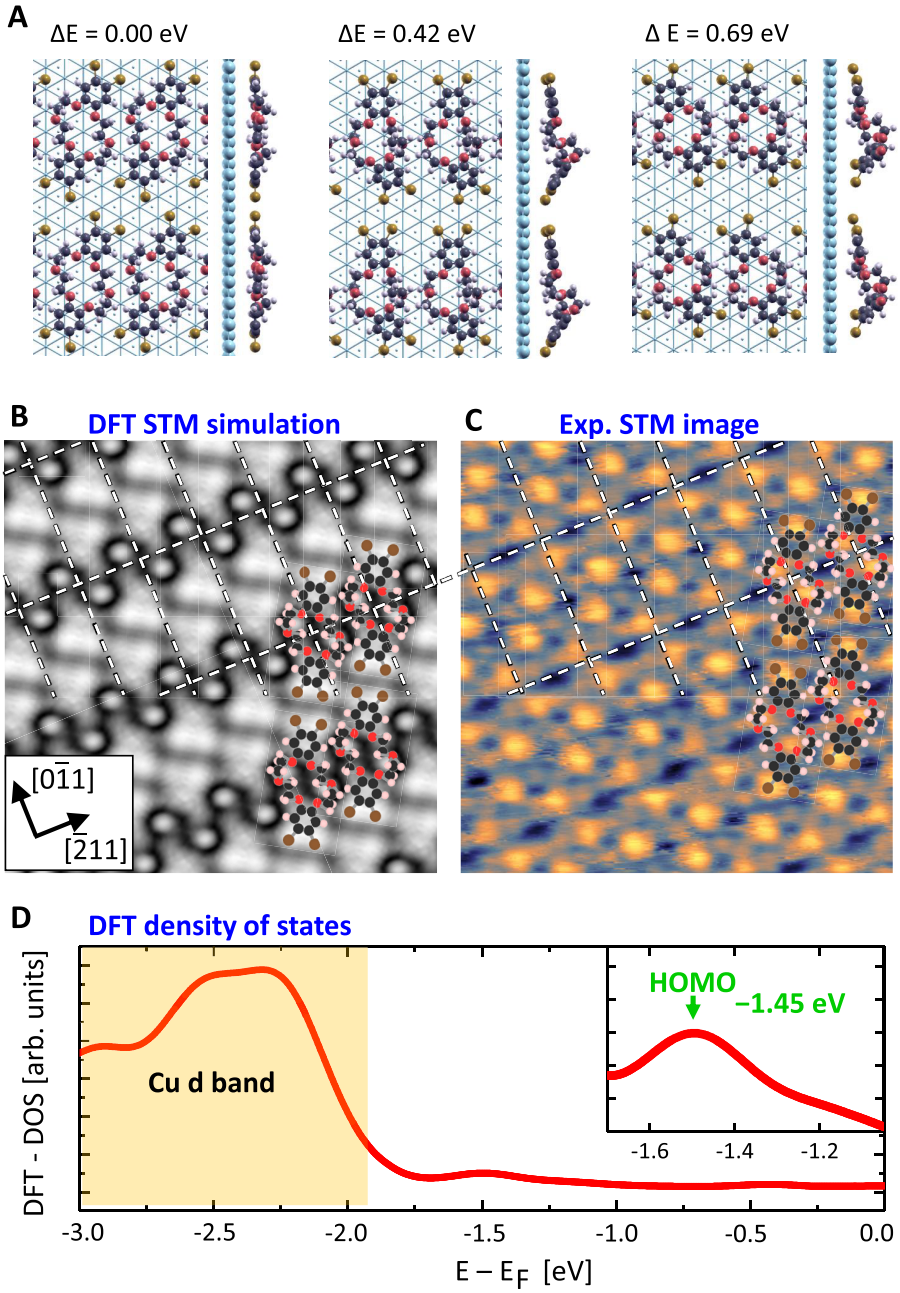

Figure 5. DFT calculations of Br-CR on Cu(111). (A) Three Br-CR two-dimensional structures on Cu(111) were tested. The structure in (A) was found to be the most energetically stable configuration: top (left) and side (right) views. For Br-CR, black, red, brown, and pink spheres denote C, O, Br, and H atoms, respectively. Hexagonal lines denote the Cu substrate lattices. (B, C) Simulated and experimentally obtained STM images at V_s = −0.7 eV (I_t = 100 pA). Two buckled carbon atoms and Br atoms are observed as bright spots. (D) Calculated DOS of Br-CR on Cu(111). The Br-CR HOMO peak is observed at −1.45 eV.

eV is observed. While there is some intensity modulation, band dispersion is not seen, indicating that intermolecular hybridization is small. The slight change of the Cu d-band shape could be due to surface scattering and different cross sections between the pristine Cu and the Br-CR coated Cu.

Angle-integrated UPS spectra for a Br-CR coverage of 0.00 ML, 0.01 ML, 0.05 ML, and 0.25 ML, obtained with $h\nu$ = 8.4 eV Xe Iα light, are shown in Figure 4C. Upon increasing the molecular coverage from 0.01 to 0.25 ML, the work function substantially decreases by 0.39 eV. The Cu(111) surface state below −0.4 eV weakens and completely vanishes at 0.25 ML coverage. At the same time the wide bump centered at −1.7 eV evolves into a sharper feature with maximum at −1.48 eV. Although the latter changes are small, we tentatively assign the peak at −1.48 eV to a molecular level of Br-CR. The HOMO peak is more clearly observed in scanning tunneling spectroscopy (STS). Figure 4D shows a dI/dV curve, which is proportional to the sample LDOS, obtained on the Br-CR island in Figure 3. All islands show identical dI/dV curves. A LDOS peak at −1.54 eV is clearly observed, while the Cu(111) surface state peak is absent (compare with the bare Cu(111) data in the inset of Figure 4D). In summary, the combined use of STS and UPS shows that upon Br-CR deposition, the work function decreases, and the Cu surface state vanishes, reflecting the formation of a continuous molecular film. At 0.25 ML

DOI: 10.1021/acs.jpcc.9b03335
J. Phys. Chem. C 2019, 123, 18939−18950

coverage, a new LDOS peak appears at −1.5 eV which we assign to a Br-CR molecular level.

3.3. DFT Calculations of Adsorbed Br-CR/Cu(111). The experimental results in Figures 1−3 show that 0.25 ML Br-CR on Cu(111) forms monolayer islands in a well-defined $\begin{pmatrix} 4 & 2 \\ 0 & 7 \end{pmatrix}$ superstructure. On the basis of these structural parameters, we have performed DFT calculations to identify the energetically stable conformation and arrangement of Br-CR on Cu(111).

Crown ethers often have several competing conformations due to the high flexibility of the crown ring.[26] In the gas phase, the free molecule is bent (see SI Figure S1F) with a calculated angle between the two benzene groups of θ = 112°. A rather small energy of 0.7 eV is needed to make the molecule flat (θ = 180°, see SI Figure S5). In the bulk crystal phase of Br-CR, the molecules have a step-like shape (SI Figure S1F). For an isolated molecule, this "stepped" conformation is 0.23 eV higher in energy than the stable "bent" conformation.

The structural optimization of the Br-CR monolayer on Cu(111) was performed in two steps. First, calculations were done for free-standing molecule layer in the same two-dimensional unit cell as the adsorbed layer $\begin{pmatrix} 4 & 2 \\ 0 & 7 \end{pmatrix}$ by starting from either the bent or the stepped conformation with several different molecular orientations. After optimization, the three most stable structures were put on the Cu(111) and optimized again. They are shown in Figure 5A. The adsorption energy of the most stable structure is −2.57 eV (see the left panel in Figure 5A). Other structures are 0.42 and 0.69 eV higher in energy (see Figure 5A). In the most stable structure, both benzene groups lie almost flat on the surface which maximizes the attractive van der Waals interaction between molecules and substrate. The crown ring is asymmetric and very different from both the bent and stepped conformation of the free molecule (see SI Figure S1F). This distortion enables the molecules to arrange themselves in a dense rectangular lattice. The two other less stable structures, have a kink, similar to the bulk stepped conformation of the Br-CR crystal (see SI Figure S5). As a result, one of the benzene groups is tilted away from the Cu surface and so the molecule−substrate interaction becomes weaker. Also, the Br atoms of neighboring molecules are farther apart than in the most energetically stable structure, thus reducing the attractive intermolecular interaction.

We have also calculated monolayers with comparable molecular density but different surface cells (5 × 5, 5 × 6, 6 × 6). The energies of these structures were found to be at least 0.22 eV higher than the stable structure shown in Figure 5A, confirming that the experimentally observed $\begin{pmatrix} 4 & 2 \\ 0 & 7 \end{pmatrix}$ arrangement affords the most stable monolayer of Br-CR on Cu(111). In the stable structure (Figure 5A), the molecule is lying very flat on the substrate and the four Br atoms are at 3.1 ± 0.1 Å above the Cu surface plane. The molecule−substrate interaction is maximized in this geometry and overcomes the energy cost (∼0.7 eV) required to "flatten" the free molecule structure (see SI Figure S5). The self-assembled monolayer structure is dictated by the delicate balance between intermolecular van der Waals and molecule−substrate interactions and the conformational flexibility of the crown ring.

Figure 5B shows the DFT STM simulation image obtained for the energetically stable flat ring structure in Figure 5A and the experimental bias. By comparing the DFT and STM images (see Figure 5B and C), the four bright protrusions observed in the STM image were identified. From Figure 5A, the Br-CR ring is flat to the Cu(111), but only two carbon atoms located at the side of the ring (see also the side view in Figure 5A) are slightly buckled from the molecule plane. Exactly at these two positions, the STM image shows two protrusions. The other two bright protrusions were found at the Br atom positions.

We further compared the DFT results with the experimentally obtained LDOS peak. Figure 5D shows the calculated DOS which is in good agreement with UPS and STS results in Figure 4. The DFT-DOS shows a peak at −1.45 eV which is mainly of Carbon-p_z orbital character and whose energy position is very close to the HOMO peak at −1.48 eV in UPS and −1.54 eV in STS. These good agreements between the theoretical and experimental results, not only for the molecular arrangements but also the LDOS peak positions, prove the high reliability of our study.

Owing to the electronic coupling between Br-CR and Cu(111), the bent structure in free-standing gas phase (see SI Figure S1F) was forced to make a flat ring, successfully producing a flat ring cavity array.

As seen from the theoretical analysis, Br-CR lies flat on Cu(111) such as the interaction between the two benzene groups and Cu is maximized. From this result, we expect that most crown ether molecules with two benzene will tend to lie flat on Cu(111), but because of the subtle balance between bending energy and adsorption energy, a bent conformation similar to the free molecule may be favored for certain molecules.

We now comment on the possibility of Br dehalogenation in our experiments. It is known that Br dehalogenation can occur at 300−400 K, but ruthenium or palladium catalytic reactions are required.[56−59] The noble metal Cu(111) surface used here is much less reactive than Ru or Pd. Further, in our study, all experiments were performed in UHV, and no catalytic reaction can happen during the sublimation process. As the C−Br bonding is rather strong and stable even at 500 K and the boiling temperature of the 1,2-dibrobenzene is 497 K, Br-CR should not be deconstructed in our experiments. We kept the crucible temperature below 400 K. Moreover, the result of SPALEED shown in Figure S7 demonstrates that the effects of the annealing on the diffraction pattern are not observed indicating any changes in the chemical structure of the molecule are hardly expected at 500 K.

3.4. Work Function Variation. We found a decrease of the work function with an increase of Br-CR deposition on Cu(111): 4.86 eV for 0 ML, 4.86 eV for 0.01 ML, 4.69 eV for 0.05 ML, and 4.47 eV for 0.25 ML (see Figure 4C). Such a decrease of the work function has been often reported for π-conjugated molecules adsorbed on coinage substrate surfaces. This is ascribed to a subtle interplay among intramolecular dipole moments, push-back effect (Pauli repulsion of metal surface electrons) and charge-transfer between the adsorbates and underlying substrates atoms. The strong push-back effect reduces a work function of coinage substrate surfaces in a range of 0.5 to 1.0 eV, while the effect is compensated by the charge-transfer interaction.[60] For the Br-CR/Cu system case, the Cu work function is continuously decreased by the depositions and the shift amount of −0.39 eV at 0.25 ML is significant and is in line with many π-conjugated molecules/metal systems reported before. This suggests that the main origin of the work function change is the push-back effect and

DOI: 10.1021/acs.jpcc.9b03335
J. Phys. Chem. C 2019, 123, 18939−18950

its compensator, i.e., charge-transfer is less effective. Indeed, the DFT calculation (see SI Figure S6B) predicts a dipole layer from the substrate to the molecular layer in the flat molecular conformation, where the intramolecular dipole moment is negligible. The DFT calculation shows that the charge transfer occurs between Br-CR and Cu(111), providing a dipole pointing normal to the surface.

4. CONCLUSIONS

We succeeded in growing a ring array using a 4,4′,5,5′-tetrabromodibenzo[18] crown-6 ether (Br-CR) molecule on an atomically flat Cu(111) substrate at 300 K, which were obtained by combined experimental studies of STM, LEED, and UPS with DFT theoretical calculation supports.

We found (1) the Br-CR ring, which is bent in bulk crystal and gas phases, becomes flat upon adsorption on Cu(111) owing to molecule−substrate electronic interactions. (2) A moderate energy balance between intermolecular and molecule−substrate interactions allows Br-CR molecule thermal diffusion on Cu(111) at room temperature, forming a well-ordered self-assembly ring array with a periodic unit of $\begin{pmatrix}\vec{a}'\\ \vec{b}'\end{pmatrix} = \begin{pmatrix}4 & 2\\ 0 & 7\end{pmatrix}\begin{pmatrix}\vec{a}\\ \vec{b}\end{pmatrix}$, where $\vec{a}$ and $\vec{b}$ denote the unit vectors on the Cu(111) substrate. (3) While the deposition of 0.05 ML Br-CR forms multidomain islands with disordered defects, a drastic improvement occurred at 0.25 ML, where only atomically flat single-domain islands were grown. This Br-CR flat ring cavity array is a promising new template for capturing guest species for making artificial array network toward the UHV on-surface based electronic devices.

■ ASSOCIATED CONTENT

Supporting Information

The Supporting Information is available free of charge on the ACS Publications website at DOI: 10.1021/acs.jpcc.9b03335.

Figure S1: UHV-STM and UHV-UPS experimental setups and the molecule evaporator with QCM rate check; Figure S2: UPS, STM atomic image, and STS surface state results obtained on the Cu(111) substrate; Figure S3: STM images of extra adsorbates on Cu(111); Figure S4: Angle-resolved UPS results; Figure S5: DFT calculations of Br−CR monolayer on Cu(111); Figure S6: UPS and DFT results of work function variation due to Br-CR adsorption on Cu(111); and Figure S7: SPALEED results of Br-CR film on Cu(111) (PDF)

■ AUTHOR INFORMATION

Corresponding Author

*E-mail: toyoyamada@faculty.chiba-u.jp (T.K.Y.).

ORCID

Peter Krüger: 0000-0002-1247-9886
Masaki Horie: 0000-0002-7734-5694
Satoshi Kera: 0000-0003-0353-5863
Toyo Kazu Yamada: 0000-0001-5185-6472

Notes

The authors declare no competing financial interest.

■ ACKNOWLEDGMENTS

This work was supported by JSPS KAKENHI Grant Number 23681018, 25110011, and 26248062, and the Asahi Glass Foundation. We thank Dr. Eiichi Inami for valuable discussions, and Dr. Takahiro Ueba and Mr. Hiroyuki Machida for supporting UPS measurements.

■ REFERENCES

(1) Tsukahara, N.; Noto, K. I.; Ohara, M.; Shiraki, S.; Takagi, N.; Takata, Y.; Miyawaki, J.; Taguchi, M.; Chainani, A.; Shin, S.; et al. Adsorption-Induced Switching of Magnetic Anisotropy in a Single Iron(II) Phthalocyanine Molecule on an Oxidized Cu(110) Surface. *Phys. Rev. Lett.* **2009**, *102*, 167203.

(2) Imada, H.; Miwa, K.; Imai-Imada, M.; Kawahara, S.; Kimura, K.; Kim, Y. Real-Space Investigation of Energy Transfer in Heterogeneous Molecular Dimers. *Nature* **2016**, *538*, 364−368.

(3) Mänz, A.; Hauke, A. A.; Witte, G. Copper Phthalocyanine as Contact Layers for Pentacene Films Grown on Coinage Metals. *J. Phys. Chem. C* **2018**, *122*, 2165−2172.

(4) Robles, R.; Lorente, N.; Isshiki, H.; Liu, J.; Katoh, K.; Breedlove, B. K.; Yamashita, M.; Komeda, T. Spin Doping of Individual Molecules by Using Single-Atom Manipulation. *Nano Lett.* **2012**, *12*, 3609−3612.

(5) Yamagishi, Y.; Nakashima, S.; Oiso, K.; Yamada, T. K. Recovery of Nanomolecular Electronic States from Tunneling Spectroscopy: LDOS of Low-Dimensional Phthalocyanine Molecular Structures on Cu(111). *Nanotechnology* **2013**, *24*, 395704.

(6) Gottfried, J. M. Surface Chemistry of Porphyrins and Phthalocyanines. *Surf. Sci. Rep.* **2015**, *70*, 259−379.

(7) Inami, E.; Shimasaki, M.; Yorimitsu, H.; Yamada, T. K. Room Temperature Stable Film Formation of π-Conjugated Organic Molecules on 3d Magnetic Substrate. *Sci. Rep.* **2018**, *8*, 353.

(8) Yamada, T. K.; Yamagishi, Y.; Nakashima, S.; Kitaoka, Y.; Nakamura, K. Role of π-d Hybridization in a 300-K Organic-Magnetic Interface: Metal-Free Phthalocyanine Single Molecules on a Bcc Fe(001) Whisker. *Phys. Rev. B: Condens. Matter Mater. Phys.* **2016**, *94*, 195437.

(9) Otero, R.; Vázquez de Parga, A. L.; Gallego, J. M. Electronic, Structural, and Chemical Effects of Charge-Transfer at Organic/Inorganic Interfaces. *Surf. Sci. Rep.* **2017**, *72*, 105−145.

(10) Pham, V. D.; Repain, V.; Chacon, C.; Bellec, A.; Girard, Y.; Rousset, S.; Abad, E.; Dappe, Y. J.; Smogunov, A.; Lagoute, J. Tuning the Electronic and Dynamical Properties of a Molecule by Atom Trapping Chemistry. *ACS Nano* **2017**, *11* (11), 10742−10749.

(11) Li, Y.; Ngo, A. T.; DiLullo, A.; Latt, K. Z.; Kersell, H.; Fisher, B.; Zapol, P.; Ulloa, S. E.; Hla, S.-W. Anomalous Kondo Resonance Mediated by Semiconducting Graphene Nanoribbons in a Molecular Heterostructure. *Nat. Commun.* **2017**, *8*, 946.

(12) Inami, E.; Yamaguchi, M.; Yamaguchi, T.; Shimasaki, M.; Yamada, T. K. Controlled Deposition Number of Organic Molecules Using Quartz Crystal Microbalance Evaluated by Scanning Tunneling Microscopy Single-Molecule-Counting. *Anal. Chem.* **2018**, *90*, 8954−8959.

(13) Lu, J.; Ruan, Z.; Guan, Y.; Bao, D. L.; Lin, X.; Hao, Z.; Zhang, H.; Song, L.; Yan, C.; Cai, J.; Du, S.; Gao, H. J. Controllable Density of Atomic Bromine in a Two-Dimensional Hydrogen Bond Network. *J. Phys. Chem. C* **2018**, *122*, 25681−25684.

(14) Garnica, M.; Stradi, D.; Barja, S.; Calleja, F.; Díaz, C.; Alcamí, M.; Martín, N.; Vázquez de Parga, A. L.; Martín, F.; Miranda, R. Long-Range Magnetic Order in a Purely Organic 2D Layer Adsorbed on Epitaxial Graphene. *Nat. Phys.* **2013**, *9*, 368−374.

(15) Esat, T.; Friedrich, N.; Tautz, F. S.; Temirov, R. A Standing Molecule as a Single-Electron Field Emitter. *Nature* **2018**, *558*, 573.

(16) Stöhr, M.; Gabriel, M.; Möller, R. Investigation of the Growth of PTCDA on Cu(110): an STM Study. *Surf. Sci.* **2002**, *507*, 330−334.

(17) Tanaka, H.; Arima, R.; Fukumori, M.; Tanaka, D.; Negishi, R.; Kobayashi, Y.; Kasai, S.; Yamada, T. K.; Ogawa, T. Method for Controlling Electrical Properties of Single-Layer Graphene Nanoribbons via Adsorbed Planar Molecular Nanoparticles. *Sci. Rep.* **2015**, *5*, 12341.

DOI: 10.1021/acs.jpcc.9b03335
J. Phys. Chem. C 2019, 123, 18939−18950

(18) Yamada, T. K.; Fukuda, H.; Fujiwara, T.; Liu, P.; Nakamura, K.; Kasai, S.; Vazquez de Parga, A. L.; Tanaka, H. Energy Gap Opening by Crossing Drop Cast Single-Layer Graphene Nanoribbons. *Nanotechnology* **2018**, *29*, 315705.
(19) Azzam, W.; Zharnikov, M.; Rohwerde, M.; Bashir, A. Functional Group Selective STM Imaging in Self-Assembled Monolayers: Benzeneselenol on Au(111). *Appl. Surf. Sci.* **2018**, *427*, 581−586.
(20) Thomas, J. C.; Goronzy, D. P.; Serino, A. C.; Auluck, H. S.; Irving, O. R.; Jimenez-Izal, E.; Deirmenjian, J. M.; Macháček, J.; Sautet, P.; Alexandrova, A. N.; Baše, T.; Weiss, P. S. Acid−Base Control of Valency within Carboranedithiol Self-Assembled Monolayers: Molecules Do the Can-Can. *ACS Nano* **2018**, *12*, 2211−2221.
(21) Machida, S.-i.; Nakayama, Y.; Duhm, S.; Xin, Q.; Funakoshi, A.; Ogawa, N.; Kera, S.; Ueno, N.; Ishii, H. Highest-Occupied-Molecular-Orbital Band Dispersion of Rubrene Single Crystal as Observed by Angle-Resolved Ultraviolet Photoelectron Spectroscopy. *Phys. Rev. Lett.* **2010**, *104*, 156401.
(22) Pedersen, C. J. Cyclic Polyethers and Their Complexes with Metal Salts. *J. Am. Chem. Soc.* **1967**, *89*, 7017−7036.
(23) Cram, D. J. The Design of Molecular Hosts, Guests, and Their Complexes. *Angew. Chem., Int. Ed. Engl.* **1988**, *27*, 1009−1020.
(24) Pedersen, C. J. The Discovery of Crown Ethers. *Science* **1988**, *241*, 536−540.
(25) Ohira, A.; Sakata, M.; Hirayama, C.; Kunitake, M. 2D-Supramolecular Arrangements f dibenzo-18-crown-6-ether and Its Inclusion Complex with Potassium Ion by Potential Controlled Adsorption. *Org. Biomol. Chem.* **2003**, *1*, 251−253.
(26) Hosokai, T.; Horie, M.; Aoki, T.; Nagamatsu, S.; Kera, S.; Okudaira, K. K.; Ueno, N. Change in Molecular Conformation of Dibenzo-Crown Ether Induced by Weak Molecule-Substrate Interaction. *J. Phys. Chem. C* **2008**, *112*, 4643−4648.
(27) Schmaltz, B.; Rouhanipour, A.; Rader, H. J.; Pisula, W.; Mullen, K. Filling the Cavity of Conjugated Carbazole Macrocycles with Graphene Molecules: Monolayers Formed by Physisorption Serve as a Surface for Pulsed Laser Deposition. *Angew. Chem., Int. Ed.* **2009**, *48*, 720−724.
(28) Kusaka, R.; Inokuchi, Y.; Ebata, T. Structure of Hydrated Clusters of Dibenzo-18-Crown-6-Ether in a Supersonic Jet-Encapsulation of Water Molecules in the Crown Cavity. *Phys. Chem. Chem. Phys.* **2008**, *10*, 6238−6244.
(29) Bruns, C. J.; Stoddart, J. F. Rotaxane-Based Molecular Muscles. *Acc. Chem. Res.* **2014**, *47*, 2186−2199.
(30) Guo, J.; Lee, J.; Contescu, C. I.; Gallego, N. C.; Pantelides, S. T.; Pennycook, S. J.; Moyer, B. A.; Chisholm, M. F. Crown Ethers in Graphene. *Nat. Commun.* **2014**, *5*, 5389.
(31) Lu, H.; Kwak, I.; Park, J. H.; O'Neill, K.; Furuyama, T.; Kobayashi, N.; Seabaugh, A.; Kummel, A.; Fullerton-Shirey, S. K. Solution-Cast Monolayers of Cobalt Crown Ether Phthalocyanine on Highly Ordered Pyrolytic Graphite. *J. Phys. Chem. C* **2015**, *119*, 21992.
(32) Cheng, S.-C.; Chen, K.-J.; Suzaki, Y.; Tsuchido, Y.; Kuo, T.-S.; Osakada, K.; Horie, M. Reversible Laser-Induced Bending of Pseudorotaxane Crystals. *J. Am. Chem. Soc.* **2018**, *140*, 90−93.
(33) Xu, K.; Lu, H.; Kinder, E. W.; Seabaugh, A.; Fullerton-Shirey, S. K. Monolayer Solid-State Electrolyte for Electric Double Layer Gating of Graphene Field-Effect Transistor. *ACS Nano* **2017**, *11*, 5453−5464.
(34) Zhang, W.; Jin, W.; Fukushima, T.; Saeki, A.; Seki, S.; Aida, T. Supramolecular Linear Hetero-junction Composed of Graphite-like Semiconducting Nanotubular Segments. *Science* **2011**, *334*, 340−343.
(35) Uoyama, H.; Goushi, K.; Shizu, K.; Nomura, H.; Adachi, C. Highly Efficient Organic Light-Emitting Diodes from Delayed Fluorescence. *Nature* **2012**, *492*, 234−238.
(36) Kim, R. H.; Kim, H. J.; Bae, I.; Hwang, S. K.; Velusamy, D. B.; Cho, S. M.; Takaishi, K.; Muto, T.; Hashizume, D.; Uchiyama, M.; Andre, P.; Mathevet, F.; Heinrich, B.; Aoyama, T.; Kim, D.; Lee, H.; Ribierre, J. C.; Park, C. Non-Volatile Organic Memory with Sub-Millimetre Bending Radius. *Nat. Commun.* **2014**, *5*, 3583.
(37) Ishii, H.; Sugiyama, K.; Ito, R.; Seki, K. Energy Level Alignment and Interfacial Electronic Structures at Organic/Metal and Organic/Organic Interfaces. *Adv. Mater.* **1999**, *11*, 605−625.
(38) Kawano, K.; Adachi, C. H. Evaluating Carrier Accumulation in Degraded Bulk Heterojunction Organic Solar Cells by a Thermally Stimulated Current Technique. *Adv. Funct. Mater.* **2009**, *19*, 3934−3940.
(39) Ma, H.; Yip, H.-L.; Huang, F.; Jen, A. K.-Y. Interface Engineering for Organic Electronics. *Adv. Funct. Mater.* **2010**, *20*, 1371−1388.
(40) Schmaus, S.; Bagrets, A.; Nahas, Y.; Yamada, T. K.; Bork, A.; Bowen, M.; Beaurepaire, E.; Evers, F.; Wulfhekel, W. Giant Magnetoresistance Through a Single Molecule. *Nat. Nanotechnol.* **2011**, *6*, 185−189.
(41) Bagrets, A.; Schmaus, S.; Jaafar, A.; Kramczynski, D.; Yamada, T. K.; Alouani, M.; Wulfhekel, W.; Evers, F. Single Molecule Magnetoresistance with Combined Antiferromagnetic and Ferromagnetic Electrodes. *Nano Lett.* **2012**, *12*, 5131−5136.
(42) Kawabe, T.; Shimose, K.; Goto, M.; Suzuki, Y.; Miwa, S. Magnetic Tunnel Junction with Fe(001)/Co Phthalocyanine/MgO(001) Single-Crystal Multilayer. *Appl. Phys. Express* **2018**, *11*, 013201.
(43) Yamada, T. K.; Abe, T.; Nazriq, N. M. K.; Irisawa, T. Electron-Bombarded <110>-Oriented Tungsten Tips for Stable Tunneling Electron Emission. *Rev. Sci. Instrum.* **2016**, *87*, 033703.
(44) Nazriq, N. K. M.; Minamitani, R.; Yamada, T. K. CO-Tip Manipulation Using Repulsive Interactions. *Nanotechnology* **2018**, *29*, 495701.
(45) Horcas, I.; Fernández, R.; Gómez-Rodríguez, J. M.; Colchero, J.; Gómez-Herrero, J.; Baro, A. M. WSXM: A Software for Scanning Probe Microscopy and a Tool for Nanotechnology. *Rev. Sci. Instrum.* **2007**, *78*, 013705.
(46) Yang, J. P.; Bussolotti, F.; Kera, S.; Ueno, N. Origin and Role of Gap States in Organic Semiconductor Studied by UPS: as the Nature of Organic Molecular Crystals. *J. Phys. D: Appl. Phys.* **2017**, *50*, 423002.
(47) Dubois, G.; Reye, C.; Corriu, R. J. P.; Chuit, C. Organic-Inorganic Hybrid Materials. Preparation and Properties of Dibenzo-18-Crown-6 Ether-Bridged Polysilsesquioxanes. *J. Mater. Chem.* **2000**, *10*, 1091−1098.
(48) Kresse, G.; Furthmuller, J. Efficient Iterative Schemes for ab initio Total Energy Calculations using a Plane-Wave Basis Set. *Phys. Rev. B: Condens. Matter Mater. Phys.* **1996**, *54*, 11169.
(49) Grimme, S. Semi-Empirical GGA-Type Density Functional Constructed with a Long-Range Dispersion Correction. *J. Comput. Chem.* **2006**, *27*, 1787.
(50) Tonigold, K.; Groß, A. Adsorption of Small Aromatic Molecules on the (111) Surfaces of Noble Metals: A Density Functional Theory Study with Semiempirical Corrections for Dispersion Effects. *J. Chem. Phys.* **2010**, *132*, 224701.
(51) Liu, W.; Ruiz, V. G.; Zhang, G. X.; Santra, B.; Ren, X.; Scheffler, M.; Tkatchenko, A. Structure and Energetics of Benzene Adsorbed on Transition-Metal Surfaces: Density-Functional Theory with Van der Waals Interactions Including Collective Substrate Response. *New J. Phys.* **2013**, *15*, 053046.
(52) Krüger, P.; Petukhov, M.; Domenichini, B.; Berko, A.; Bourgeois, S. Monolayer Formation of Molybdenum Carbonyl on Cu(111) Revealed by Scanning Tunneling Microscopy and Density Functional Theory. *J. Phys. Chem. C* **2012**, *116*, 10617−10622.
(53) Krüger, P.; da Pieve, F.; Osterwalder, J. Real-Spaces Multiple Scattering Method for Angle-Resolved Photoemission and Valence-Band Photoelectron Diffraction at Its Application to Cu(111). *Phys. Rev. B: Condens. Matter Mater. Phys.* **2011**, *83*, 115437.
(54) Nakashima, S.; Yamagishi, Y.; Oiso, K.; Yamada, T. K. How Contacting Electrode Affect Single π-Conjugated Molecular Electronic States: Local Density of States of Phthalocyanine Nanomolecules on MgO(001), Cu(111), Ag(001), Fe(001), and Mn(001). *Jpn. J. Appl. Phys.* **2013**, *52*, 110115.

DOI: 10.1021/acs.jpcc.9b03335
J. Phys. Chem. C 2019, 123, 18939−18950

(55) Schwoebel, R. L.; Shipsey, E. J. Step Motion on Crystal Surfaces. *J. Appl. Phys.* **1966**, *37*, 3682−3686.
(56) Zhong, H.; Liu, C.; Zhou, H.; Wang, Y.; Wang, R. Prefunctionalized Porous Organic Polymers: Effective Supports of Surface Palladium Nanoparticles for the Enhancement of Catalytic Performances in Dehalogenation. *Chem. - Eur. J.* **2016**, *22*, 12533−12541.
(57) You, T.; Wang, Z.; Chen, J.; Xia, Y. Transfer Hydro-Dehalogenation of Organic Halides Catalyzed by Ruthenium(II) Complex. *J. Org. Chem.* **2017**, *82*, 1340−1346.
(58) Sabater, S.; Mata, J. A.; Peris, E. Hydrodefluorination of Carbon-Fluorine Bonds by The Synergistic Action of a Ruthenium-Palladium Catalyst. *Nat. Commun.* **2013**, *4*, 2553.
(59) Guo, X.; Yu, C.; Yin, Z.; Sun, S.; Seto, C. T. Hydrodehalogenation of Polyhalogenated Aromatics Catalyzed by NiPd Nanoparticles Supported on Nitrogen-Doped Graphene. *Chem. Sus. Chem.* **2018**, *11*, 1617−1620.
(60) Duhm, S.; Gerlach, A.; Salzmann, I.; Broker, B.; Johnson, R. L.; Schreiber, F.; Koch, N. PTCDA on Au(111), Ag(111) and Cu(111): Correlation of Interface Charge Transfer to Bonding Distance. *Org. Electron.* **2008**, *9*, 111.

DOI: 10.1021/acs.jpcc.9b03335
J. Phys. Chem. C 2019, 123, 18939−18950